

Electronic Supplementary Information for: **Silica Supported Ruthenium Oxide Nanoparticulates as Efficient Catalysts for Water Oxidation**

Yang Zhang, and Tong Ren*

Department of Chemistry, Purdue University, 560 Oval Drive, West Lafayette, Indiana 47907

The Supporting Information section includes:

Fig. S1 TEM image of as-synthesized $\text{RuO}_2 \cdot x\text{H}_2\text{O}$ NPs.

Fig. S2 (a) Nitrogen sorption isotherms of NP-4% and SBA-15, and (b) the corresponding pore size distributions, and the results discussion.

Fig. S3 Small angle XRD patterns of **NP-4%** and SBA-15.

Fig. S4 TEM image of **RuCl₃-4%** featuring crystallized RuO₂ on the surface of SBA-15.

Fig. S5 Wide angle XRD pattern of NP @ silica spheres, in comparison with the patterns of **NP-4%** and calcined NP + SBA-15.

Fig. S6 The Ce(IV) consumption rate of NP @ silica spheres compared to that of NP-4%.

Fig. S7 The residual [Ce(IV)] (%) over time at the fifth cycle of reaction, catalyzed by unsupported RuO₂ NPs.

Table S1 TOF values calculated based on original reaction conditions, and the calculation details and further analysis of the kinetic data of samples reported in Table 1.

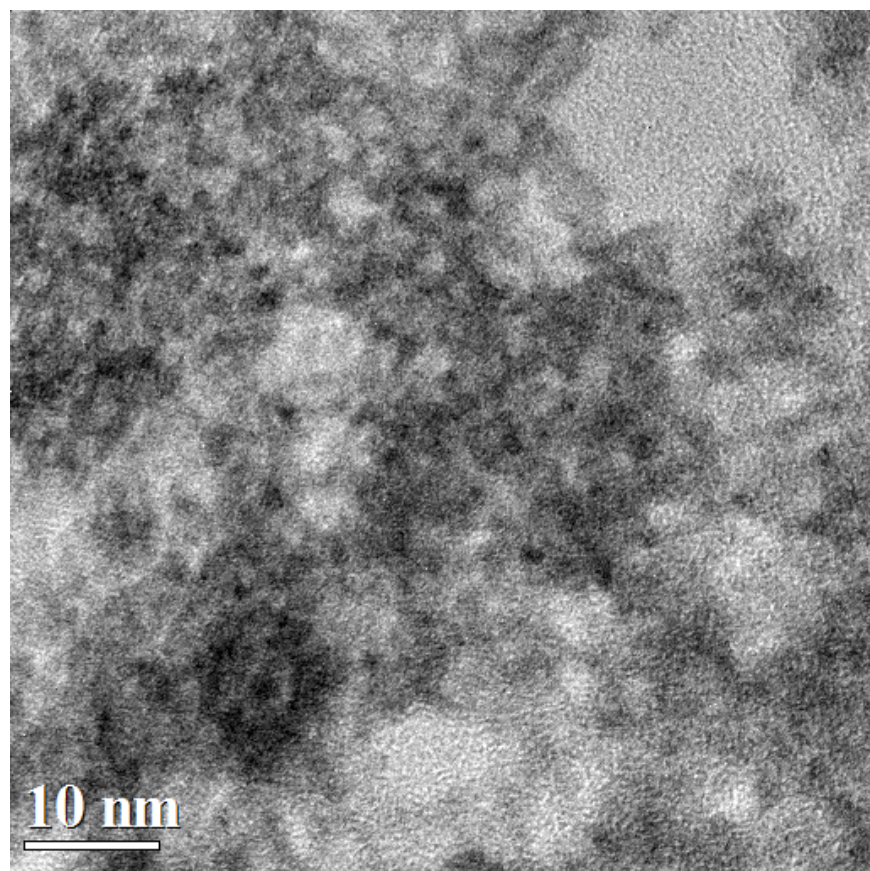


Fig. S1 TEM image of as-synthesized $\text{RuO}_2\text{•}x\text{H}_2\text{O}$ NPs.

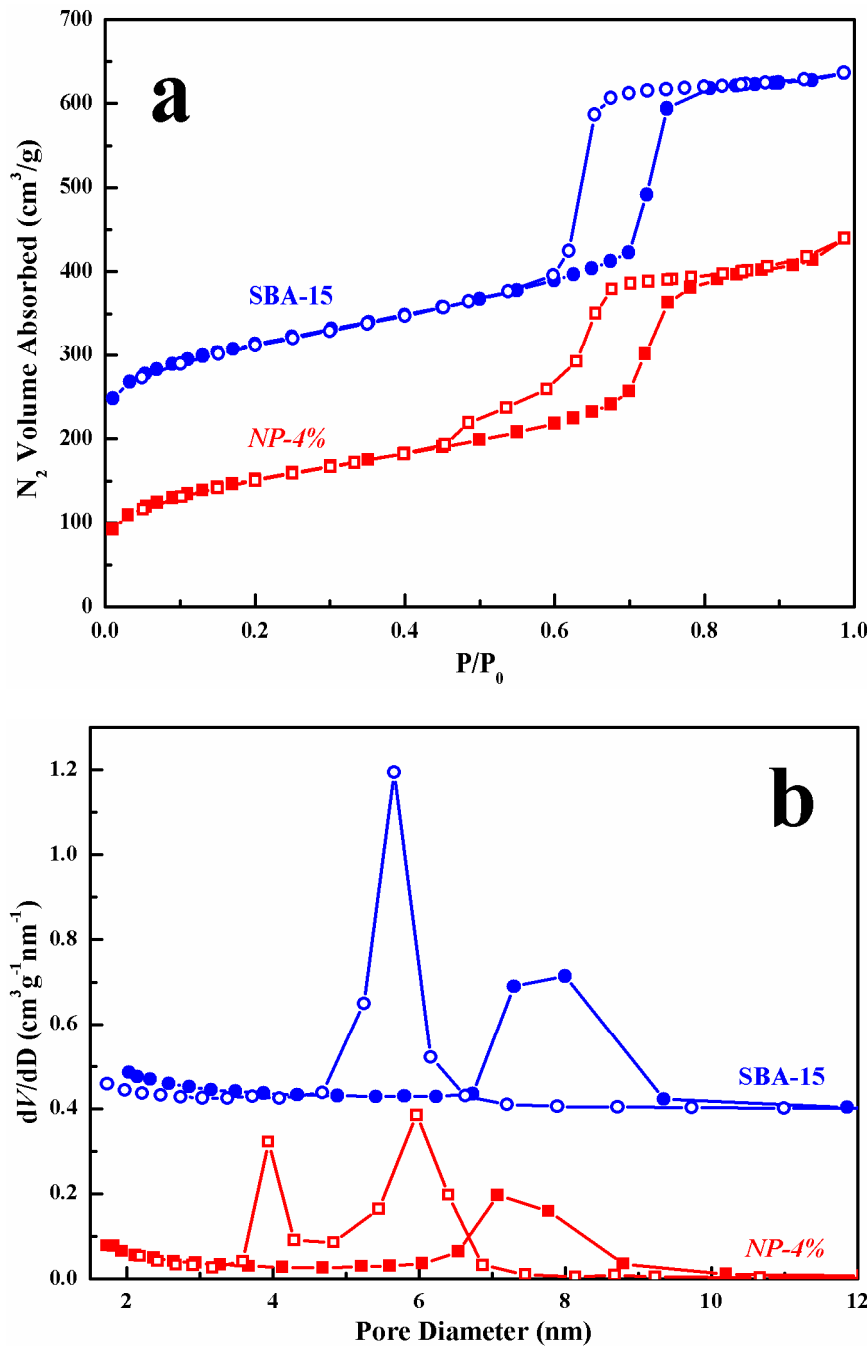


Fig. S2 (a) Nitrogen sorption isotherms of NP-4% and SBA-15, and (b) the corresponding pore size distributions (1.7 nm - 12 nm) calculated from adsorption (solid) and desorption (hollow) branches *via* the Barrett-Joyner-Halenda (BJH) method. The isotherm of SBA-15 is offset vertically by $150 \text{ cm}^3 \text{g}^{-1}$ and the pore distribution of SBA-15 is offset by $0.4 \text{ cm}^3 \text{g}^{-1} \text{nm}^{-1}$.

N_2 adsorption-desorption isotherms (Fig. S2a) of NP-4% and SBA-15 both exhibit type-IV curves, representative of mesoporous materials. Only SBA-15 exhibits a standard H_1 hysteresis loop; NP-4% differs from SBA-15 in the desorption branch at $P/P_0 = 0.45\text{-}0.6$, where the convergence of adsorption and desorption branches is delayed. The hysteresis loop is also different from typical H_2 type in which a single steep desorption at relatively low pressure results from narrow entrances to the internal pores. It therefore suggests that the internal channels, instead of the entrances, were locally narrowed by the loaded nanosized RuO_2 , which hindered the evaporation of adsorbed nitrogen inside during desorption. In Fig. S2b, the pore size calculated from the adsorption branch of NP-4% and SBA-15 is centered at 7.4 nm and 7.6 nm, respectively. Estimated from the desorption branch of NP-4%, additional distribution appears around 4-5 nm representing the narrowed “neck”, which is 1-2 nm smaller than the most probable diameter at 6 nm in both SBA-15 and NP-4%, coinciding with the size of original NPs. The specific area of NP-4% is $531 \text{ m}^2\text{g}^{-1}$, 92% of SBA-15 ($575 \text{ m}^2\text{g}^{-1}$), while the pore volume is $0.68 \text{ cm}^3\text{g}^{-1}$, 91% of SBA-15 ($0.75 \text{ cm}^3\text{g}^{-1}$). The small reduction of surface contact and porosity of the mesoporous carrier reveals no significant pore blockage due to the loaded NPs, critical for the retention of catalytic activities.

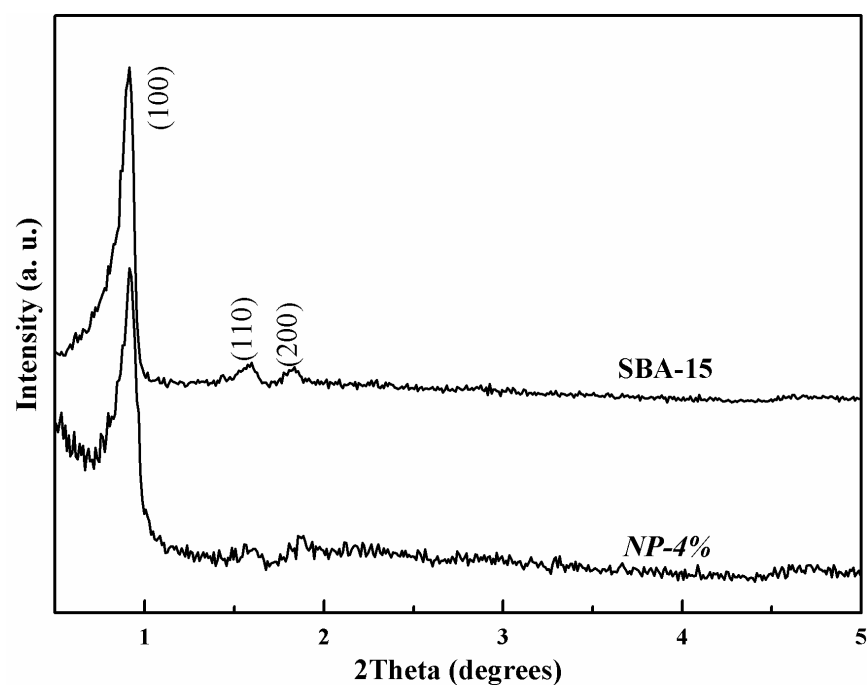


Fig. S3 Small angle XRD patterns of **NP-4%** and **SBA-15**.

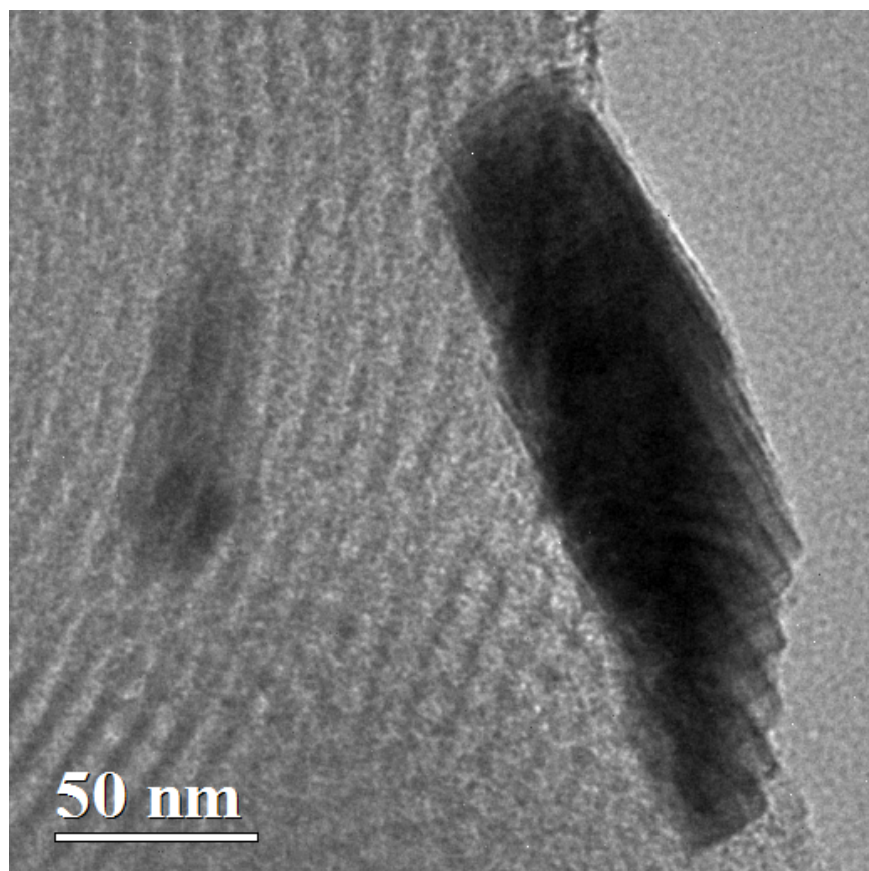


Fig. S4 TEM image of **RuCl₃-4%** featuring crystallized RuO₂ on the surface of SBA-15.

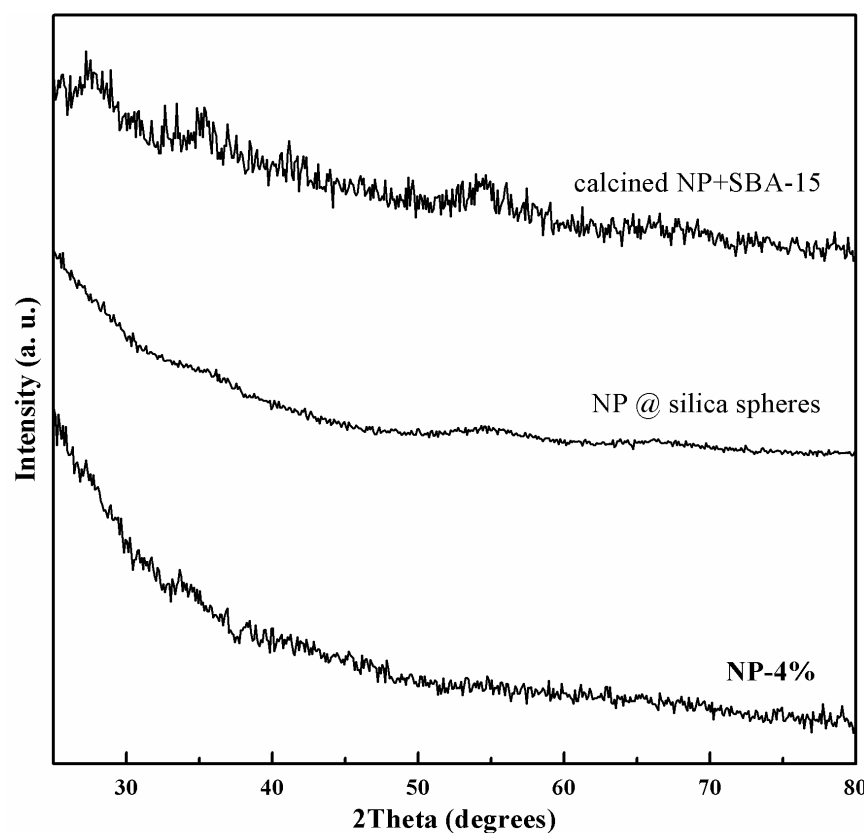


Fig. S5 Wide angle XRD pattern of NP @ silica spheres (RuO₂ NPs supported on silica colloidal spheres), in comparison with the patterns of **NP-4%** and calcined NP + SBA-15. The silica spherical particles were prepared with a modified Stöber method.¹ Briefly, 9.8 mL 20 wt% ammonia, 73.8 mL ethanol and 10.8 mL deionized water were mixed together. Then 5.6 mL tetraethyl orthosilicate (TEOS) was added into the solution at once. The mixture was kept stirring for 12 h. The colloids were centrifuged and re-dispersed with pure ethanol for 4 times, and then centrifuged and dispersed with H₂O until the pH of the solvent reaches ~ 7. The colloids were then centrifuged and dried, and then used as the support for NPs. The preparation of NP @ silica spheres was similar to that of **NP-4%**, by dispersing and mixing 4 wt% of NPs and 96 wt% of the silica spheres in water, evaporating the solvent, and then calcining at 350 °C for 4h.

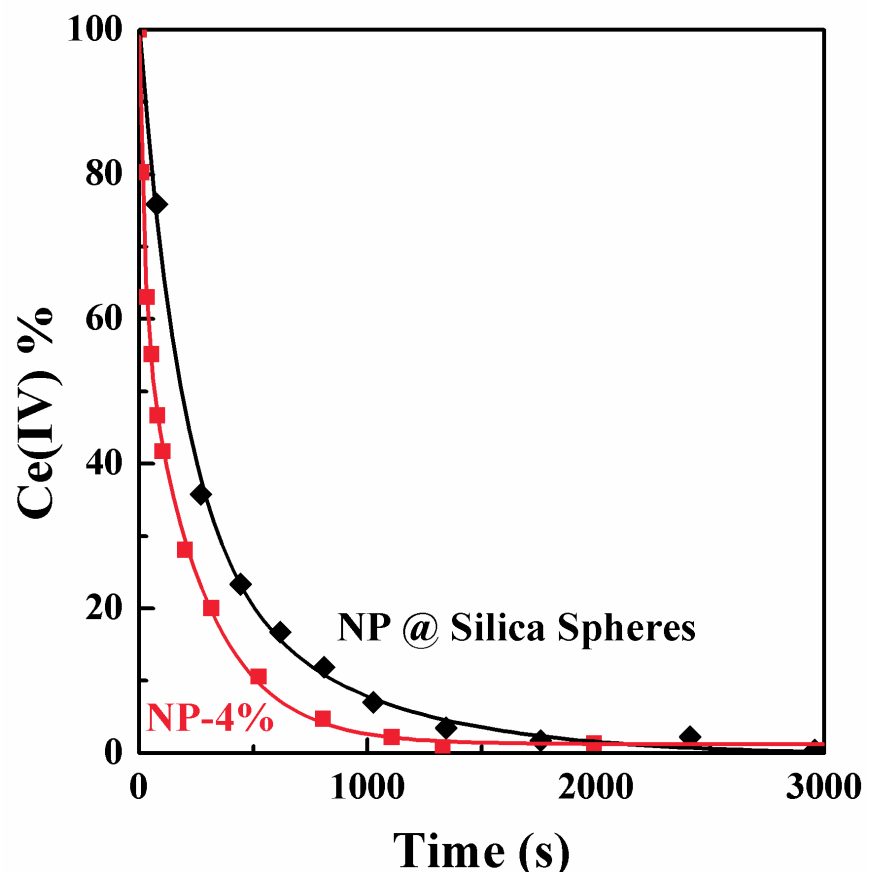


Fig. S6 The Ce(IV) consumption rate of NP @ silica spheres compared to that of NP-4%.

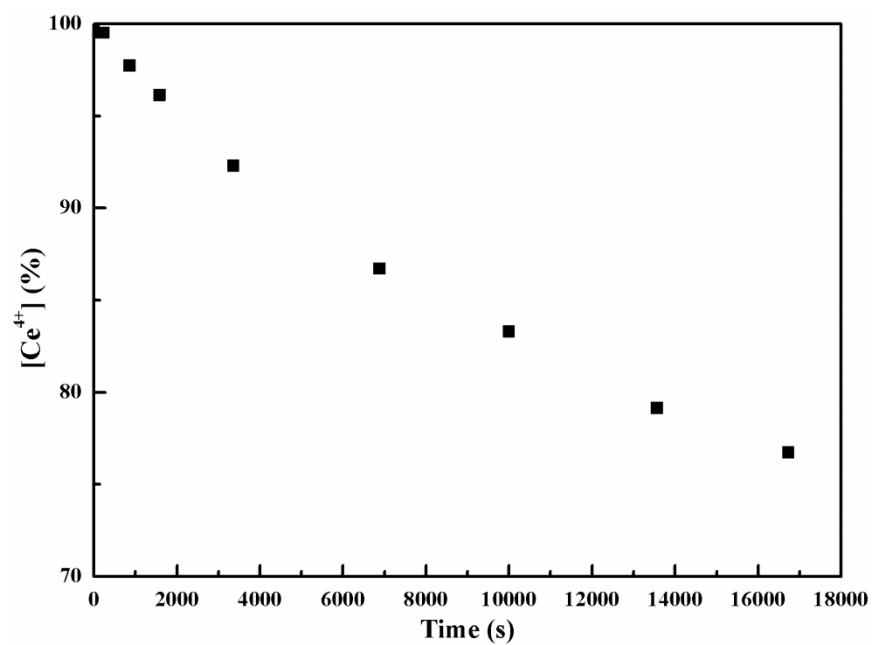


Fig. S7 The residual [Ce(IV)] (%) over time at the fifth cycle of reaction, catalyzed by unsupported RuO₂ NPs.

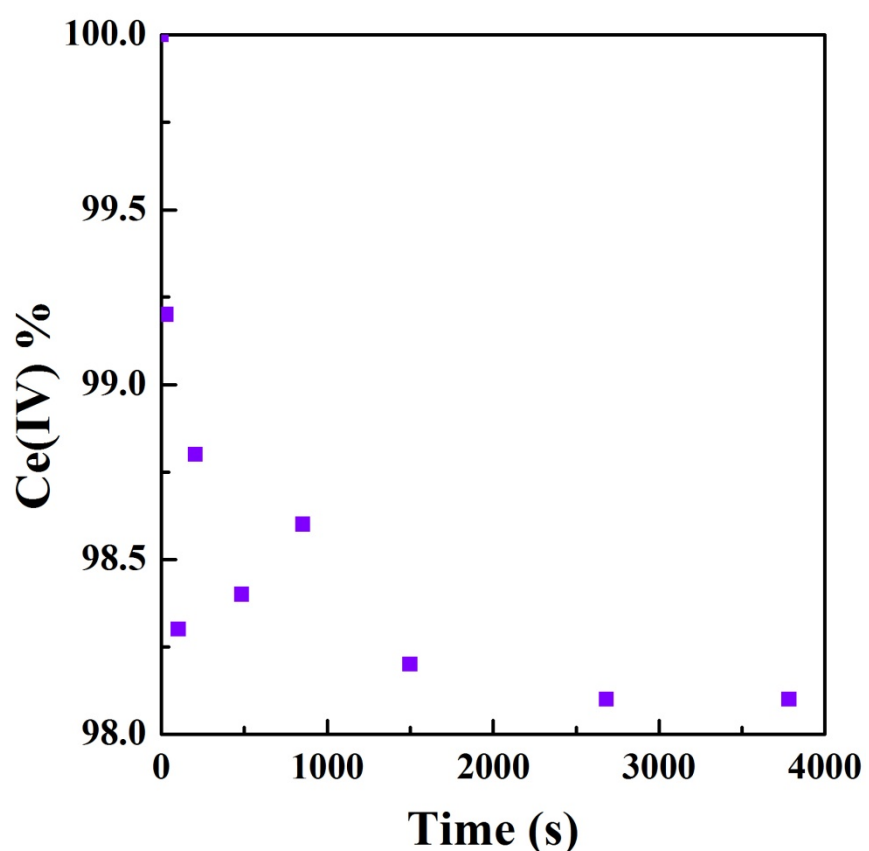


Fig. S8 In the control update experiment of Ce^{4+} with SBA-15 without catalyst, the loss of absorbance of Ce^{4+} over time. Within one hour the loss is <2%, which is within the error range of UV-vis measurement.

Calculation and further analysis of the kinetic data of samples reported in

Table 1.

The preliminary kinetic study of the reaction catalyzed by **NP-4%** showed that the reaction was not first-order towards [Ce(IV)], different from the samples cited in Table 1 for comparison. Therefore, a comparison of first-order rate constant k_1 is meaningless. Besides, because in different report the concentration of the catalyst varied, the rate constants cannot be directly compared. The comparison of turnover number (TON) during certain period is not the best choice either, due to the different kinetics (non-first-order reaction) of [Ce(IV)] disappearance in different examples. Therefore the comparison of initial TOF, which directly indicates the activity of catalyst, is more empirical.

The initial TOFs of the catalytic reactions shown in Table S1 was calculated as follows: In most reports the kinetic study of water oxidation can obtain first-order rate constant k_1 , towards the disappearance of Ce(IV). The concentration of catalytic RuO₂ ([RuO₂]) in the solution and the initial concentration of Ce(IV) ([Ce(IV)]_{t=0}) can also be found. The equation of TOF is:

$$\text{TOF} = \frac{-k_1(s^{-1}) \times [\text{Ce(IV)}]_{t=0}(\text{M})}{[\text{RuO}_2](\text{M})}$$

For instance, in a reference ² we found $k_1 = -6.5 \times 10^{-3} \text{ s}^{-1}$, $[\text{Ce(IV)}]_{t=0} = 1 \times 10^{-3} \text{ M}$, and $[\text{RuO}_2] = 3.41 \times 10^{-4} \text{ M}$, and thus obtained $\text{TOF} = 0.019 \text{ s}^{-1}$.

Table S1 TOF values calculated based on original reaction conditions.

Sample	TOF (s ⁻¹)	k ₁ (s ⁻¹)	[Ce(IV)] _{t=0} (mM)	Ref
NP-4%	0.27	-	2	-
	0.053	-	1	
Ru-Adam(500)	0.024	0.015	0.92	³
RuO ₂ •yH ₂ O	0.016	0.0099	0.92	³⁻⁵
RuO ₂ -loaded mesoporous silicate	0.019	0.0065	1	²
RuO ₂ on TiO ₂ ^a	~0.01	~0.0008	1	⁶

^aIn the report of RuO₂ loaded on TiO₂, no detailed kinetic study was provided, and therefore we estimated the TOF based on Fig. 3 of their report.⁶

The abovementioned calculation method directly compared TOFs in the original reaction conditions and is therefore most reliable. However, the obtained TOF values depend on the initial concentration of Ce⁴⁺. Since most of the reported reactions are first-order to [Ce(IV)], within a reasonable range the TOF is linear to the initial concentration of Ce(IV). To exclude the influence of [Ce(IV)]_{t=0}, we set all the [Ce(IV)]_{t=0} values to 2×10^{-3} M. For the reaction catalyzed by RuO₂-loaded TiO₂,⁶ the reaction was assumed as first-order with respect to [Ce(IV)], and the thus-calculated rate constant in 1×10^{-3} M Ce(SO₄)₂ is used to calculate the TOF in 2×10^{-3} M Ce(SO₄)₂. The results were summarized in Table 1 of the main text.

References

1. W. Stober and A. Fink, *J. Colloid. Interface Sci.*, 1968, **26**, 62-69.
2. N. C. King, C. Dickinson, W. Zhou and D. W. Bruce, *Dalton Trans.*, 2005, 1027-1032.
3. A. Mills and T. Russell, *J. Chem. Soc., Faraday Trans.*, 1991, **87**, 1245-1250.
4. A. Mills and S. Giddings, *Inorg. Chim. Acta*, 1989, **158**, 49-57.
5. A. Mills, *Chem. Soc. Rev.*, 1989, **18**, 285-316.
6. A. Mills, P. A. Duckmanton and J. Reglinski, *Chem. Commun.*, 2010, **46**, 2397-2398.